Organic Electronics 13 (2012) 1827–1835

Contents lists available at SciVerse ScienceDirect

Organic Electronics

journal homepage: www.elsevier.com/locate/orgel

On the exciton profile in OLEDs-seamless optical and electrical modeling

B. Perucco [a,*], N.A. Reinke [a], D. Rezzonico [b], E. Knapp [a], S. Harkema [c], B. Ruhstaller [a,b]

[a] Zurich University of Applied Sciences (ZHAW), Institute of Computational Physics, Technikumstrasse 9, 8400 Winterthur, Switzerland
[b] Fluxim AG, Dorfstrasse 7, 8835 Feusisberg, Switzerland
[c] Holst Centre, High Tech Campus 31, 5656 AE Eindhoven, The Netherlands

ARTICLE INFO

Article history:
Received 15 April 2011
Received in revised form 4 May 2012
Accepted 12 May 2012
Available online 15 June 2012

Keywords:
Simulation
Exciton profile
Emission profile
Parameter extraction
Organic light-emitting devices

ABSTRACT

We present a comprehensive model to simulate organic light-emitting devices (OLEDs) that includes a seamless coupling of charges, excitons and photons. The comprehensive model accounts for the position dependent exciton lifetime due to the optical environment in the multilayer OLED structures. We first study the effect of different charge mobilities and quantum efficiencies of the light-emitting material on the exciton profiles. Moreover, we discuss the extension of an optical model to account for the exciton dynamics. This comprehensive optical model is validated and justified on the basis of consistency checks. Namely, we show that our comprehensive optical model can take the cavity effects as seen in simulation results of the comprehensive electrical model into account. The advantage of the comprehensive optical model is a quick and accurate insight into the exciton physics if applied together with a nonlinear least square (NLSQ) fitting method. Finally, we apply the comprehensive optical model with the NLSQ-method in order to extract the exciton profiles from emission spectra of a blue light-emitting polymer diode (PLED) measured at different current levels.

1. Introduction

Organic light-emitting devices (OLEDs) are being commercialized in novel lighting and flat-planel display applications. For these applications, high efficiency, long lifetime and low cost are essential. Therefore, it is of huge interest to increase the lifetime and understand the mechanisms that contribute to light-outcoupling in an OLED. For example, the light outcoupling efficiency can be enhanced by recovering the surface plasmon modes by index coupling, prism coupling and grating coupling [1–3]. A thick electron transport layer as a spacer to an electrode on top of a high-index substrate can also achieve high outcoupling efficiencies [4]. Further, it was shown by simulation that the orientation of the dipoles, as well as the quantum efficiency of the emitter, play an important role on the outcoupling efficiency [5–8]. Moreover, to observe the internal features of the dipole radiation in the OLED far-field, devices with adapted layer structure are needed to optically enhance the feature of interest [9]. The motivation of our paper is to achieve an accurate description of the exciton profile in the light-emitting layer. On the one hand, we aim for a more accurate calculation of the exciton profile with a comprehensive electrical model. On the other hand, a comprehensive optical model allows for improved outcoupling efficiency predictions and a more accurate extraction of exciton profiles. We use a dipole model where the emitted power is calculated from a given shape of the exciton profile. It is common to assume exciton profiles with a Gaussian or exponential shape [10]. The exponential shape for the exciton profile can be derived as the steady-state solution of the exciton continuity equation with a delta-dirac generation term and a constant exciton decay time [11]. A draw-back of an approach with analytical exciton profiles is that the influence of the optical cavity typically observed in multilayer OLED structures is neglected. The cavity changes the power emitted to the different decay

* Corresponding author.
E-mail address: benjamin.perucco@zhaw.ch (B. Perucco).

1566-1199/$ - see front matter © 2012 Elsevier B.V. All rights reserved.
http://dx.doi.org/10.1016/j.orgel.2012.05.053

channels as a function of the position. Thus, it causes a change of the exciton lifetime, especially near metallic interfaces the lifetime is decreased considerably, and therefore, the shape of the resulting exciton profile in general is changed. We demonstrate an approach to study this effect by solving the charge drift–diffusion equations of holes and electrons for the multilayer OLED structure. By introducing an exciton continuity equation with a position dependent radiation rate, we account for the influence of the cavity on the excitons. A second motivation of our paper is to provide a useful and quick analysis tool to get insight into the distribution of excitons in an OLED. This is achieved by accounting for the position dependent exciton dynamics in the optical model. Then for extraction of exciton profiles from measured data, we minimize the error between the simulated and measured emission spectra by a nonlinear least-square method. Approaches, where least-square methods were used to determine the shape of the exciton profile were also discussed recently by several authors [12–18].

The paper is organized in the following way. In Section 2, we introduce the different optical and electrical device models studied in this paper. Section 3 briefly introduces a nonlinear least-square (NLSQ) method for the extraction of exciton profiles from spectral and angular data. Section 4 presents a consistency check where the optical and electrical device models are validated. Finally in Section 5, we apply the NLSQ-method to emission spectra of a PLED which were measured at different current levels. This application demonstrates the impact of the NLSQ-method in combination with the comprehensive optical model for studying the influence of different operating conditions on the exciton profile.

2. Modeling methods

In this section, we present the models to simulate the light outcoupling of OLEDs by seamlessly taking electrons, excitons and photons into account. The first model we discuss is the optical model. As depicted in Fig. 1, the optical model is used to calculate the light-outcoupling of an OLED. In a next step, we introduce the comprehensive electrical model, where we solve the charge drift–diffusion equations for holes and electrons. The hole and electron profile determine the recombination profile as illustrated in the flow-chart diagram in Fig. 1. By coupling the optical model to the diffusion and decay of the excitons, we account for the optical feedback of the cavity of a multilayer OLED structure. The exciton profile then is taken to calculate the light-outcoupling by the optical model. This is called the bottom-up approach or electrical simulation. Finally, we derive the comprehensive optical model to account for the exciton dynamics. This is called the top-down approach or optical simulation.

2.1. Optical model

The optical model describes light-outcoupling of an organic light-emitting device. The foundation of the model was set by Sommerfeld [19] by describing the impact of

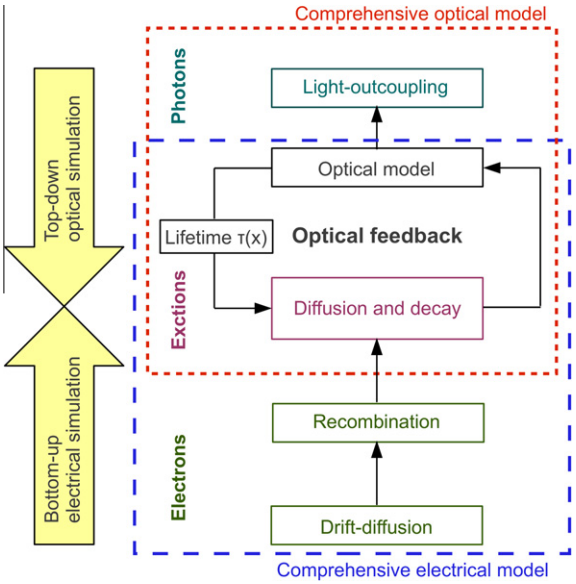

Fig. 1. Flow-chart diagram of the models to calculate light-outcoupling of an OLED.

an interface on electromagnetic radiation of a dipole. The model was enhanced by Chance et al. by considering reflection at two interfaces [20]. Other authors further improved the model by calculating also light-emission outside of the multilayer interfaces [21,22]. The model characterizes the influence of nearby multilayer interfaces on the radiation of fluorescent molecules, which are naturally described as oscillating dipoles. It is assumed that a dipole has two decay channels, namely radiative decay k_r and nonradiative decay k_{nr}. The model relates the total decay rate in presence of multilayer interfaces $k = k_r + k_{nr}$ to the total decay rate in an infinite medium $k_0 = k_{r,0} + k_{nr}$. Throughout the paper, all intrinsic quantities are denoted by the subscript 0. 'Intrinsic' means in absence of the multilayer interface. The nonradiative decay channel k_{nr} is not influenced by the multilayer interfaces, therefore we do not distinguish between a nonradiative decay in absence or presence of multilayer interfaces. The dipole model reads

$$\frac{k}{k_0} = P_{\mathrm{rel}}, \tag{1}$$

where P_{rel} stands for the relative change in the dissipated power of a dipole by the multilayer interfaces compared to the infinite medium. The power is a complex integral depending on the wavelength λ and position x of the dipole in the emissive layer. In order to obtain the emission spectra generated by a dipole in the emissive layer, one has to solve the Helmholtz equations for the electric field [20,21]. Considering the illustration in Fig. 2, modes starting out in the emission zone pass the interfaces 12 and 13 and reach the region 2 and 3. Passing the interfaces 12 and 13 results in a partial absorption or reflection of the emitted radiation. Calculating the Poynting vector from the electric field allows the determination of the relative power $F(\theta,\lambda,x)$

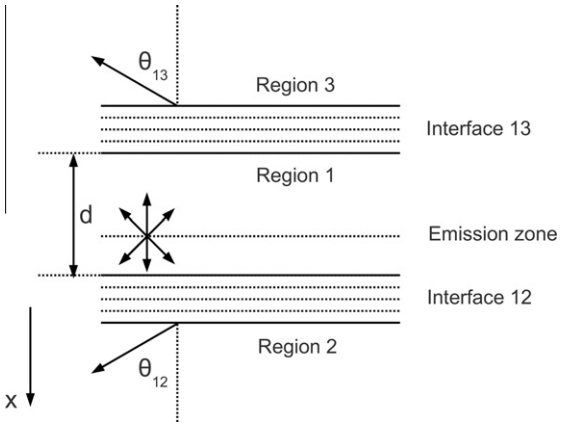

Fig. 2. A multilayer structure is depicted schematically. Region 1 is the emissive layer with thickness d and region 2 and 3 are semi-infinite, non-absorbing media. The emission zone where the dipoles are placed is drawn as a single position. The multilayer interfaces are entitled as interface 12 and 13. The emission angles θ_{12} and θ_{13} are defined in region 1, respectively region 3, where an angle of 0° is perpendicular to the interface plane and an angle of 90° is parallel to the interface.

entering region 2 and 3 provided the regions can be treated as non-absorbing media. The relative power $F(\theta,\lambda,x)$ is also a function of the angle θ of the outcoupled light as depicted in Fig. 2. It is unlikely that only a single dipole at a single position contributes to the light-emission. Often, the emission zone or exciton profile (the distribution of the dipoles within the emissive layer) in an OLED has a well confined shape, typically approximated by Gaussian or exponential function [10]. For thin emissive layers in small molecule OLEDs, a constant exciton profile can be a good first approximation, too [23]. Even the most simple recombination profile (delta-dirac) leads to an exponential exciton profile [11]. An exciton can be interpreted as a bound state of a hole and electron and is physically treated as an oscillating dipole in the optical model. Therefore, we introduce $S(x)$ to define the exciton profile as a function of the position in the emissive layer. We model the emission spectrum $E(\lambda,\theta)$ of an OLED as

$$E(\lambda,\theta) = k_0 \cdot q_0 \cdot \int_I F(\theta,\lambda,x) \cdot S(x) \cdot dx, \tag{2}$$

where the quantum efficiency q_0 is defined as $q_0 = k_{r,0}/(k_{r,0} + k_{nr})$. The integration is performed over the emissive layer I. Throughout the paper, for the discretization dx typically 1 nm is assumed. Eq. (2) can alternatively be written as

$$E(\lambda,\theta) = k_{r,0} \cdot \int_I F(\theta,\lambda,x) \cdot S(x) \cdot dx. \tag{3}$$

Because we scale the relative power $F(\theta,\lambda,x)$ emitted by a single dipole into region 2 and 3 with the radiative decay rate $k_{r,0}$, we obtain the absolute power radiated by the dipole. Multiplying the absolute power of a single dipole by the exciton profile $S(x)$ yields a power density.

2.2. Comprehensive electrical model

In Section 2.1, we have assumed that the exciton profile $S(x)$ defining the emission zone is known a priori. Another approach to obtain the emission zone is to solve the charge drift–diffusion and exciton transport equations for the organic semiconductor [24–26]. The drift–diffusion equations are continuity equations for holes and electrons, which are injected into the device at the anode, respectively the cathode. We assume electrons and holes to recombine according to the Langevin recombination rate $R(x)$, which is proportional to

$$R(x) \propto (\mu_p + \mu_n) \cdot p(x) \cdot n(x). \tag{4}$$

The mobility of the electrons and holes is denoted as μ_n and μ_p. The electron density $n(x)$ and hole density $p(x)$ are both solutions to the charge drift–diffusion equations. The mobilities are material parameters and must be determined by measurement. We take generation, diffusion and decay of excitons into account by writing the continuity equation in steady-state as

$$\nabla \cdot (-D \cdot \nabla S(x)) = G \cdot R(x) - \frac{S(x)}{\tau(x)}. \tag{5}$$

The term $-D \cdot \nabla S(x)$ describes the exciton diffusion current driven by a gradient in the density of excitons. $G \cdot R(x)$ is the generation of excitons by Langevin recombination and G is a Langevin recombination prefactor that is set to 0.25 for creation of singlet excitons. $S(x)/\tau(x)$ is the decay of excitons by radiative and nonradiative decay. The lifetime $\tau(x)$ can be written as $\tau(x) = 1/k(x) = 1/(k_r(x) + k_{nr})$ and must be calculated with the optical dipole model as presented in Section 2.1. By solving Eq. (5), we obtain $S(x)$ which is afterwards inserted into Eq. (3) to calculate the emission spectrum. In Fig. 3a, we see the relative power emitted into the different optical decay channels. The power emitted originates from a single emission zone and is a function of the relative position in the light-emitting polymer (LEP) material. The structure of the OLED is illustrated in Fig. 4 and the dipoles are assumed to be isotropically distributed. To perform the mode analysis, a wavelength of 588 nm, a quantum efficiency of $q_0 = 1$ and a lifetime of $\tau_0 = 10$ ns is chosen. The calculations were performed with the software SETFOS [27]. The best outcoupling efficiency of approximately 12% is achieved by excitons near the center of the LEP material. Due to coupling of excitons to evanescent and surface plasmon modes, the exciton lifetime $\tau(x)$ is very short near the electrodes as seen in Fig. 3b. The position dependent lifetime in Eq. (5) and Fig. 3b is calculated according to the dipole emission model of Chance et al. [20] by

$$\tau(x) = \frac{1}{k(x)} = \frac{\tau_0}{1 - q_0 \cdot \int_0^\infty f(x,u)\ \mathrm{d}u}. \tag{6}$$

Eq. (6) describes the effect of the cavity on the dipole lifetime, which can be written as $\tau_0 = 1/k_0 = 1/(k_{r,0} + k_{nr})$. $f(x,u)$ is a measure of the dipole relaxation time and u is the normalized inplane wave vector. The lifetime is only constant $\tau(x) = \tau_0$ in case of $q_0 = 0$. Then, the cavity has no influence on the decay rate of excitons because nonradiative decay

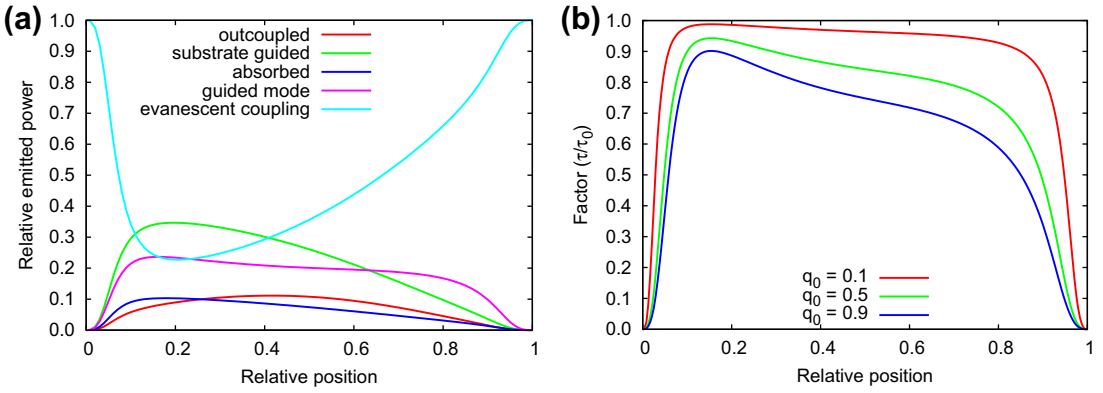

Fig. 3. (a) Relative emitted power into the different optical decay channels as a function of the position of the isotropic dipoles in the emissive layer calculated by SETFOS. The wavelength taken for the calculation is 588 nm. The device considered in the analysis is a typical PLED presented in Fig. 4 and the relative position is measured from the anode ($q_0 = 1$, $\tau_0 = 10$ ns). (b) The spatial lifetime as a function of different intrinsic quantum efficiencies q_0. The lifetime τ is normalized by the intrinsic lifetime τ_0.

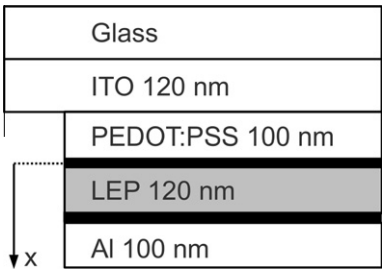

Fig. 4. A typical multilayer structure of a PLED used for the consistency checks. The light-emitting polymer (LEP) layer is embedded between the anode and cathode, indicated by the black layers. Therefore, we model a single-layer device.

dominates and coincidentally, this situation would result in no light emission. For $q_0 > 0$, the influence of the optical environment becomes apparent, see Fig. 3b. In the case where $q_0 = 0.1$, the influence of the cavity is only present near the electrodes. In the central region in the LEP layer, the lifetime is almost unaffected. But for $q_0 > 0.5$, the lifetime τ is reduced considerably with respect to the intrinsic lifetime τ_0. The comprehensive electrical model accounts seamlessly for electrons, excitons, and photons, and the optical environment.

2.3. Comprehensive optical model

The empirical factor $\tau(x)/\tau_0$ contains spatial information about the exciton lifetime. If the exciton lifetime is very short $\tau(x)/\tau_0 \approx 0$, less contribution to light-emission is made by excitons at this position. If the exciton lifetime is high $\tau(x)/\tau_0 \approx 1$, more excitons contribute to light-emission at this position. The comprehensive optical model can be written as

$$E_c(\lambda,\theta) = k_{r,0} \cdot \int_I F(\theta,\lambda,x) \cdot S_c(x) \cdot dx. \tag{7}$$

Eq. (7) is different to Eq. (3) because it uses a different exciton profile $S_c(x)$. It is a corrected version of the exciton profile $S(x)$ originally assumed in Eq. (3). Motivated in the text above, the exciton profile $S_c(x)$ is calculated as

$$S_c(x) = \tau(x)/\tau_0 \cdot f \cdot S(x). \tag{8}$$

The empirical factor $\tau(x)/\tau_0$ influences the emitted power in absolute quantities. Therefore, we introduce a scaling-factor f, which has to be determined by comparison to experiment as we will present in Section 3. The lifetime $\tau(x)$ can be obtained by applying Eq. (6) and requires knowledge of the quantum efficiency q_0. Flämmich et al. demonstrated that it is feasible to extract the intrinsic quantum efficiency by layer-thickness dependent optical measurements [28]. The comprehensive optical model is crosschecked in Section 4.2 by the comprehensive electrical model in order to justify the weighting factor $\tau(x)/\tau_0$.

3. Nonlinear least-square fitting method

We use a nonlinear least-square (NLSQ) fitting method to extract the exciton profile $S_c(x)$ from measured emission spectra. The shape of the exciton profile $S(x)$ is approximated by an analytical function determined by two parameters, the peak position p and the width w of the exciton profile. We minimize the χ^2 error

$$\chi^2 = \frac{1}{2NM}\left(\sum_{s,p}\sum_{j}^{M}\sum_{i}^{N}\left(E^{s,p}_{\mathrm{calc}}(\lambda_i,\theta_j,p,w,f) - E^{s,p}_{\mathrm{ref}}(\lambda_i,\theta_j)\right)^2\right)^{\frac{1}{2}} \tag{9}$$

between the calculated emission spectra $E^{s,p}_{\mathrm{calc}}$ and measured emission spectra $E^{s,p}_{\mathrm{ref}}$ with respect to the fit parameters p, w and f. s and p denote s-polarized and p-polarized light. The emission spectra are a function of wavelength λ_i and emission angle of the outcoupled light θ_j. N is the number of different wavelengths in the emission spectrum and M is the number of different angles in the emission spectrum. The division by $2NM$ is used to calculate an averaged χ^2 error in order to compare it to situations where different number of measured emission intensities are used. The NLSQ-method estimates the peak position p, the width

w and the scaling factor f to obtain the exciton distribution $S_c(x)$.

4. Consistency checks

4.1. Electrical simulation

In a series of consistency checks we calculate the emission spectra of an OLED based on the comprehensive electrical model by seamlessly considering charges, excitons, and photons. For the consistency checks, we choose three device configurations that differ in the assumed charge mobilities and thus yield different recombination and exciton profiles. Unlike a previous publication [26], we do not consider a Gaussian disorder model here for simplicity.

Thus, the molecular orbital energies have a discrete level. We model the device as a single-layer device where the charges are injected at the electrodes by thermionic injection. The structure of the device is depicted in Fig. 4. Other device and simulation parameters can be found in Table 1. By varying the constant mobilities of holes and electrons as illustrated in Table 2, we tune where the peak of the exciton profile is located within the light-emitting polymer (LEP). The mobilities are selected so that in one configuration the peak of the exciton profile is close to the anode (case 1), respectively in another configuration the peak of the exciton profile is close to the cathode (case 3). In a third situation, the mobilities are balanced so that the exciton profile is symmetrical (case 2). We reference the different mobilities of holes and electrons later as cases 1–3, see Table 2. In Section 2.2, we argued that q_0 can be interpreted as a turn-on parameter for the cavity effects in the emissive layer. We study the effect of q_0 on the calculated exciton profiles from the comprehensive electrical model. We select three different quantum efficiencies $q_0 = 0.1$, $q_0 = 0.5$, and $q_0 = 0.9$ as already used in Fig. 3(b). In Fig. 5a, the calculated electron and hole profiles for an applied voltage of 11 V are plotted. The three different colors represent the three different cases for the charge mobilities. The dashed lines are the hole profiles and the solid lines are the electron profiles. The position in the LEP layer is defined with respect to the PEDOT:PSS interface and is expressed in terms of a relative position. We see that holes are injected on the anode side, whereas the electrons are injected on the cathode side. In the case where both electron and hole mobility are equal (case 2), the hole and electron profiles are symmetrical. In the other situations (case 1 and case 2), the charge profiles are asymmetrical. From the electron and hole profiles one derives the recombination profile. The recombination profiles are depicted in Fig. 5b for the three different cases for the charge mobilities. As expected, we see a symmetrical profile where the electron and hole mobility are balanced and an asymmetrical profile where the electron mobility is higher than the hole mobility, and vice versa. Once the recombination profiles $R(x)$ are determined, we obtain the exciton profile by solving the continuity equation of the excitons (see Eq. (5)). The exciton profiles for the different mobility cases and different quantum efficiencies are shown in Fig. 6a–c as symbols. We observe a peak shift of the exciton profile when varying the mobilities for electrons and holes. The influence of the optical environment on the exciton profile leads to a situation where no excitons are physically present at the electrodes in steady-state. Further, we see the stronger the influence of the cavity, the smaller the amount of excitons present in the emissive layer as the whole profile is reduced by increasing quantum efficiency. In fact, this is compensated by the increased intrinsic radiative decay rate $k_{r,0}$ that goes along with increasing the quantum efficiency. So total emitted power by the excitons is raised with higher quantum efficiency q_0. It can also be seen that various quantum efficiencies slightly lead to a shift in the peak position for every mobility case. In the paper, we do not depict all the calculated emission spectra from the different exciton profiles as seen in Fig. 6a–c. In Fig. 7a and c, we show a representative example of the calculated emission spectra for the mobility case 2 (balanced electron and hole mobility) and a quantum efficiency of 0.5.

Table 1
Device and simulation parameters assumed in order to calculate the exciton profiles in the LEP layer.

Parameter	Description	Value
ϵ_r	Relative permeability	3.2
G	Recombination factor	0.25
L	Diffusion length	20 nm
HOMO	HOMO level	5.4 eV
LUMO	LUMO level	2.4 eV
N_0	Density of states	$1 \cdot 10^{27}$ m^{-3}
τ_0	Lifetime	10 ns
Φ_a	Workfunction anode	5.2 eV
Φ_c	Workfunction cathode	2.6 eV

Table 2
Mobility parameters for calculating the exciton profiles where the peak is close to the anode side (case 1), in the center of the emissive layer (case 2) and close to the cathode side (case 3). μ_n is the electron and μ_p the hole mobility. Both mobilities are assumed constant.

Case	μ_n (m^2/(Vs))	μ_p (m^2/(Vs))
1	2×10^{-9}	1×10^{-9}
2	2×10^{-9}	2×10^{-9}
3	1×10^{-9}	2×10^{-9}

4.2. Extraction of exciton profiles – a consistency check

In a next step we apply the NLSQ-method to extract the exciton profile from the emission spectra calculated by the comprehensive electrical model. The NLSQ-method tunes the parameters p, w and f of the comprehensive optical model so that the χ^2 error is minimized. A Gaussian shape of the exciton profile is chosen as it is a very simple mathematical function that can describe both narrow and broad exciton profiles, without loss of generality. From the estimated parameters p, w and f, we calculate the exciton profile $S_c(x)$. By cross-checking it with the reference exciton profile from the electrical model S_{ref}, we validate and justify the approach to include information about the optical environment by the factor $\tau(x)/\tau_0$ in the comprehensive optical model. Thereby, we obtain a physically accurate estimate of the exciton profile as it would result from a bottom-up electrical calculation or as it would occur in a real device. As a representative illustration

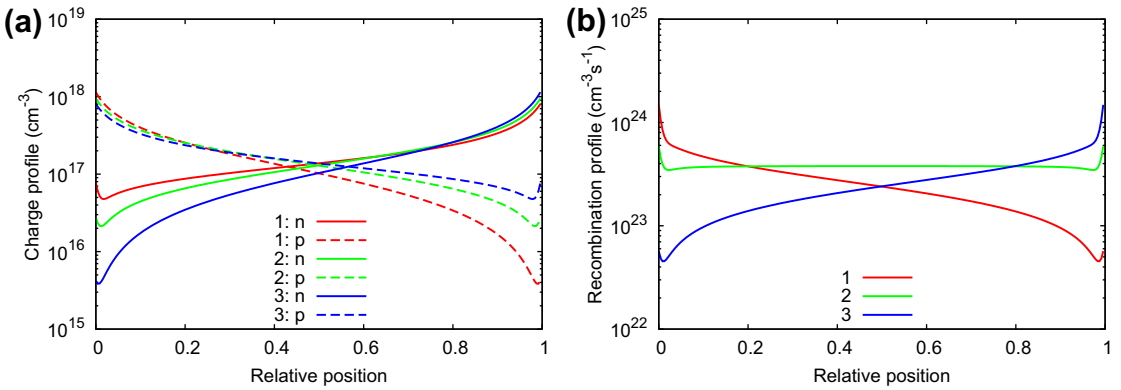

Fig. 5. (a) Charge profiles for electrons (solid line) and holes (dashed lines) for different cases of the mobility parameters (see Table 2) as a function of the relative position in the emissive layer. Zero corresponds to the anode side and 1 to the cathode side. In case 1, the electron mobility is higher than the hole mobility, in case 3 it is vice versa. Case 2 represents balanced hole and electron mobilities. (b) Obtained recombination profiles from the charge profiles by applying Eq. (4).

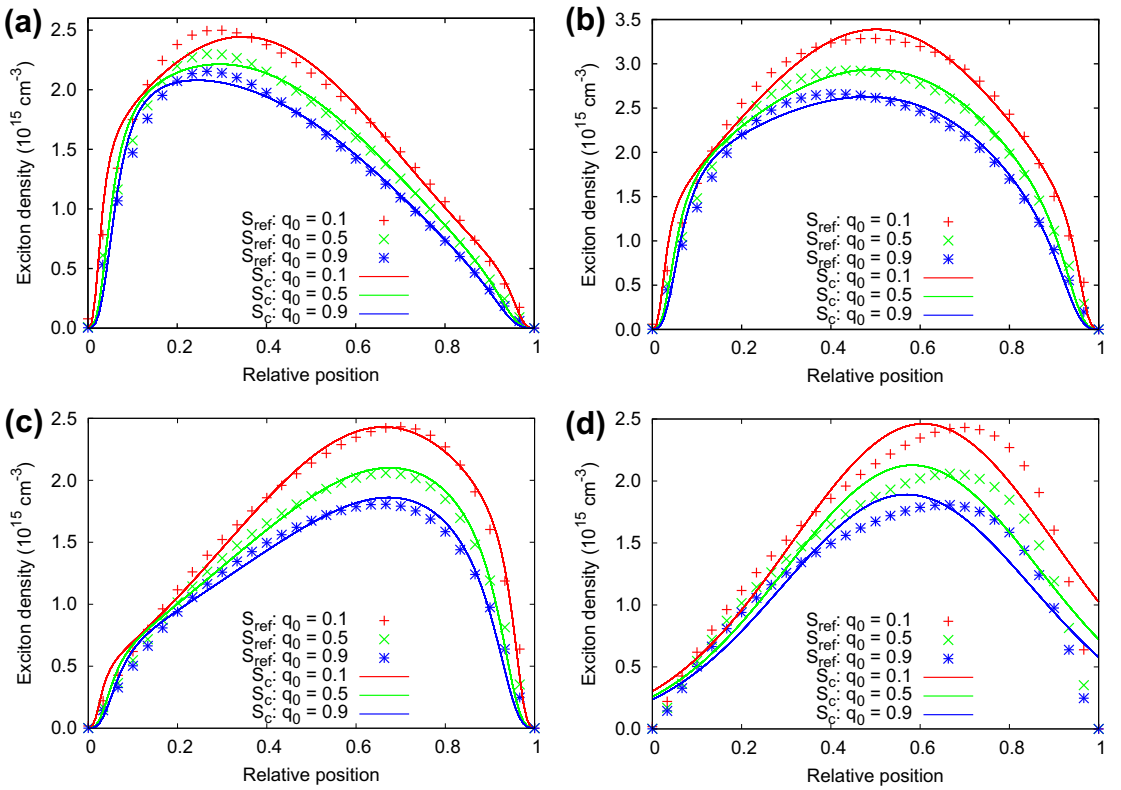

Fig. 6. Comparison between reference and extracted exciton profiles for various quantum efficiencies and charge mobilities. The reference exciton profiles are the result of the comprehensive electrical model. (a) In this situation the electron mobility is higher than the hole mobility. (b) In this case, both charge mobilities are balanced. (c) It is assumed that the hole mobility is higher than the electron mobility for this situation. The extracted exciton profiles are based on the comprehensive optical model in (a–c). For case 3 in (d), the optical model is used to extract the exciton profiles.

of the fit quality, Fig. 7a–d show the comparison between the reference and fitted emission spectra for the case where the charge mobilities are balanced (case 2) and $q_0 = 0.5$. Fig. 7a and c depict the reference emission spectra for s-polarized and p-polarized light. Fig. 7b and d illustrate the corresponding fitted emission spectra for the s-polarized and p-polarized light. Fig. 7a–d prove that the fit is excellent. The relative error between the reference and fitted emission spectra is 0.3 ‰. In Fig. 7, the emission spectra are normalized by the highest intensity value obtained in the reference s-polarized and p-polarized emission spectra, respectively. The optical simulation results of the emission spectra in Fig. 7 do not include birefrigence and show the emission spectra in the glass substrate. The corresponding extracted exciton profiles for the

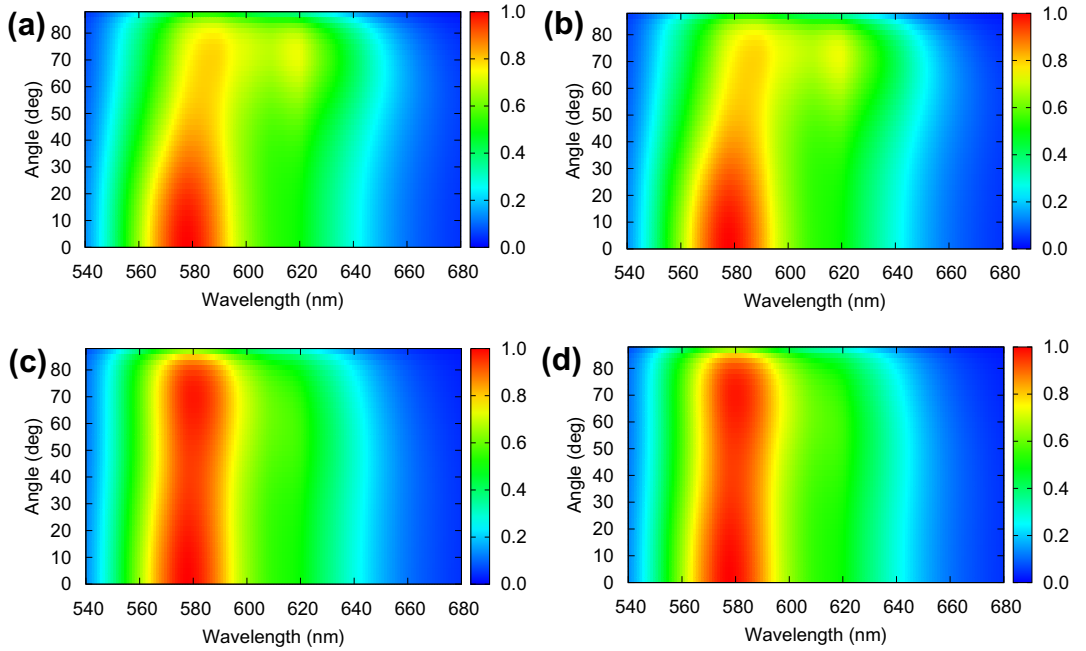

Fig. 7. Comparison between the reference and fitted emission spectra. The reference emission spectra are depicted in (a) for the s-polarized light and in (c) for the p-polarized light. The fitted emission spectra are shown in (b) for the s-polarized light and in (d) for the p-polarized light. The reference emission spectra are calculated using balanced charge mobilities and a quantum efficiency of 0.5. The emission spectra are normalized by the highest intensity value obtained in the reference s-polarized and p-polarized emission spectra, respectively. The relative error with respect to the intensity between the reference and fitted emission spectra is 0.3‰ and indicates a perfect fit.

various cases (different settings in the charge mobilities) are found in Fig. 6a–c and are represented by lines. The calculated exciton profiles from the electrical simulation are drawn with symbols. The exciton profiles $S_c(x)$ agree well with the reference exciton profiles regardless of the mobility cases and intrinsic quantum efficiencies. The shape of the exciton profile is reproduced independently from the location of the peak position and width of the exciton profile. Also in its absolute quantities, the exciton profiles are reconstructed. As a comparison for the case 3, Fig. 6d shows the extracted exciton profiles if we used the optical model instead of the comprehensive optical model. It shows differences to the reference exciton profiles especially near the electrodes where the influence of the cavity is more pronounced. Therefore, from the very good agreement demonstrated in Fig. 6a–c, we can justify our $\tau(x)/\tau_0$ weighting approach in the comprehensive optical model. We see that the factor $\tau(x)/\tau_0$ of the comprehensive optical model accurately estimates the exciton profile from the reference simulation by a single optical least-square fitting approach. The advantage of the comprehensive optical model in combination with the NLSQ-method is the physically meaningful shape of the obtained exciton profile, taking into account the optical influence of the cavity.

5. Determination of exciton profiles based on measured emission spectra

In Section 4.2 we demonstrated that the NLSQ-method in combination with the comprehensive optical model is able to reproduce the reference exciton profiles. In this section, we want to apply the method to measured emission spectra of a blue-emitting PLED based on a copolymer that was previously reported by Harkema et al. [29]. The copolymer analyzed here was referred to as copolymer 2 in reference [29]. PLEDs with this copolymer deliver luminous efficiency up to 7 cd/A. For the fit, the emission spectra between wavelengths λ from 440 nm to 580 nm and viewing angles θ between 0° and 60° were taken into account. The viewing angle represents θ_{13} as depicted in Fig. 2. The PLED's structure is a 175 nm thick blue light-emitting polymer (LEP, copolymer 2) embedded between the aluminum cathode and the ITO anode. The exact structure of the device with an area of 9 mm^2 is as follows: ITO (135 nm)/LEP (175 nm)/Ag (60 nm). We study the exciton profiles as a function of the current, therefore, the emission spectra are measured at different currents at 0.2 mA, 0.5 mA, 1.0 mA and 2.0 mA. In order to apply the NLSQ-method, we have to make some assumptions about the orientation of the dipoles and the analytical shape of the exciton profile, as well as the initial values parameterizing that shape. The dipoles are assumed to be oriented horizontally. For the shape of the exciton profile, a Gaussian distribution is chosen and its initial peak position is set to 0.2, meaning the peak is shifted to the anode in the LEP material. The initial width is set to 32 nm. Another assumption is the intrinsic quantum efficiency q_0 and lifetime τ_0. The quantum efficiency $q_0 = 0.55$ for this copolymer was previously determined by a photoluminescence experiment in an integrating sphere by Harkema et al. [29] and the lifetime τ_0 is set to 10 ns. The selection of the lifetime τ_0 does not affect the shape of the extracted exciton profiles as the $\tau(x)$ scales with τ_0 (see

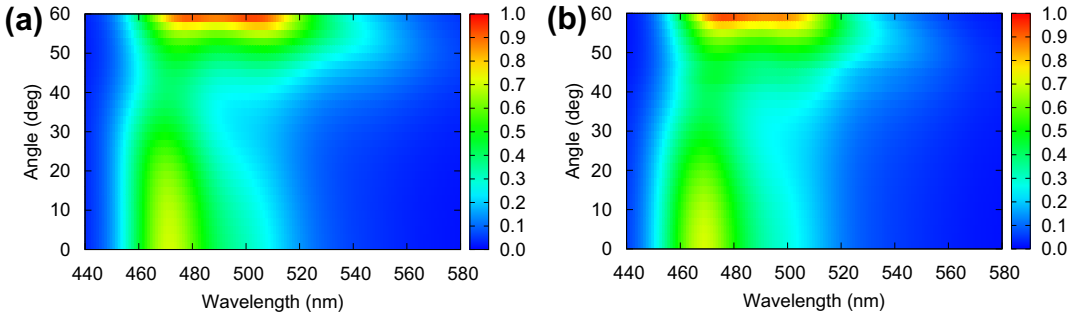

Fig. 8. Representative illustration of the fit quality for a structure of ITO (135 nm)/LEP (175 nm)/Ag (60 nm). The emission spectra were generated by driving the device at a current of 1.0 mA. The measured emission spectra is depicted in (a) and the fitted emission spectra are shown in (b). The emission intensity values are normalized by the highest value obtained in the experiment or simulation, respectively. The assumed intrinsic quantum efficiency and lifetime is set to $q_0 = 0.55$ and $\tau_0 = 10$ ns. The relative error with respect to the intensity between the reference and fitted emission spectra is 12.8 %.

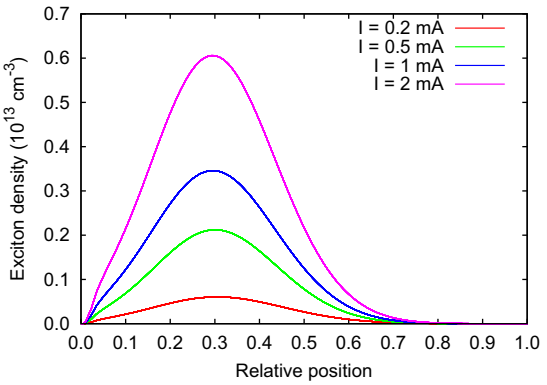

Fig. 9. Extracted exciton profiles by the NLSQ-method for different currents of the PLED device. When increasing the current, the total amount of excitons in the emissive layer is increased and there is no shift of the peak position observed. For a current of 1.0 mA, the corresponding measured and fitted emission spectra are shown in Fig. 8.

Eq. (6)) and is compensated by the scaling factor f to fit the emission spectra in absolute intensities. Fig. 8a–b show a representative comparison between the measured and fitted emission spectra using the NLSQ-method when the device is driven at a current of 1.0 mA. The simulated emission spectra match the experiment accurately. The emission spectra are normalized by the highest intensity value obtained in the measurement or simulation, respectively. The extracted emission profiles are depicted in Fig. 9. There is no shift observed of the peak position with increasing current, only the total amount of excitons present in the LEP layer is increased at higher current. The higher the current that drives the device, the more holes and electrons are injected at the electrodes. Therefore, the number of excitons is also increased. This application illustrates the practical and quick use of the comprehensive optical model for getting an accurate insight into the electrical transport processes and optical phenomena by fitting emission spectra.

6. Conclusion

In summary, we presented a comprehensive electrical device model which considers the charge drift–diffusion and recombination equations as well as the exciton continuity equation. By coupling the dipole model of Chance et al. to the continuity equation of excitons, accurate exciton profiles are calculated taking the effect of the cavity on the exciton dynamics into account. In a second step, we modified the dipole model to the comprehensive optical model by a factor $\tau(x)/\tau_0$ stating where the lifetime of the excitons is reduced due to coupling to evanescent and surface plasmon modes. For fitting the comprehensive optical model parameters, we applied a nonlinear least-square (NLSQ) fitting method. The weighting factor $\tau(x)/\tau_0$ in the comprehensive optical model is validated and justified by comparing the extracted exciton profiles $S_c(x)$ to the exciton profile resulting from the electrical simulation. The extracted exciton profiles $S_c(x)$ describe the reference exciton profile not only qualitatively by their shape but also fit the reference exciton profiles in terms of the absolute amount of excitons present in the emissive layer. To demonstrate an application of the comprehensive optical model in combination with the NLSQ-method, we applied the method to measured emission spectra of a blue-emitting PLED. The emission spectra were measured for different current densities through the PLED. Our comprehensive electrical model which seamlessly couples charges, exciton and photons is also suitable for small-molecule OLEDs in order to predict an accurate shape of the exciton profile. In addition, the nonlinear least-square fitting method in combination with the comprehensive optical model can be applied for in situ studies of aging mechanisms in OLEDs by only measuring the emission spectra. Moreover, the comprehensive optical model and the fitting algorithm will facilitate the validation of electrical device models.

Acknowledgement

We appreciate fruitful discussions regarding parameter extraction with Andor Bariska from the Institute of Data Analysis and Process Design (ZHAW), Switzerland. Financial support through the European FP7 project AEVIOM.eu under Grant No. 213708 is gratefully acknowledged.

References

[1] J. Frischeisen, Q. Niu, A. Abdellah, J.B. Kinzel, R. Gehlhaar, G. Scarpa, C. Adachi, P. Lugli, W. Brütting, Light extraction from surface plasmon and waveguide modes in an organic light-emitting layer by nanoimprinted gratings, Optics Express 19 (S1) (2011) A7–A19.

[2] J. Frischeisen, B.J. Scholz, B.J. Arndt, T.D. Schmidt, R. Gehlhaar, C. Adachi, W. Brütting, Strategies for light extraction from surface plasmons in organic light-emitting diodes, J. Photon. Energy. 1 (2011) 011004.

[3] G. Gaertner, H. Greiner, Light extraction from OLEDS with (high) index matched glass substrates, Proc. SPIE 6999 (2008) 69992T.

[4] S. Mladenovski, K. Neyts, D. Pavicic, A. Werner, C. Rothe, Exceptionally efficient organic light emitting devices using high refractive index substrates, Optics Express 17 (9) (2009) 7562–7570.

[5] J. Frischeisen, D. Yokoyama, C. Adachi, W. Brütting, Determination of molecular dipole orientation in doped fluorescent organic thin films by photoluminescence measurements, Appl. Phy. Let. 96 (2010) 073302.

[6] M. Flämmich, M.C. Gather, N. Danz, D. Michaelis, A.H. Bräuer, K. Meerholz, A. Tünnermann, Orientation of emissive dipoles in OLEDs: quantitative in situ analysis, Org. Electron. 11 (6) (2010) 1039–1046.

[7] B.C. Krummacher, S. Nowy, J. Frischeisen, M. Klein, W. Brütting, "Efficiency analysis of organic light-emitting diodes based on optical simulation, Org. Electron. 10 (3) (2009) 478–485.

[8] S. Nowy, B.C. Krummacher, J. Frischeisen, N.A. Reinke, W. Brütting, "Light extraction and optical loss mechanisms in organic light-emitting diodes: Influence of the emitter quantum efficiency, J. Appl. Phys. 104 (2008) 123109.

[9] M. Flämmich, J. Frischeisen, D.S. Setz, D. Michaelis, B.C. Krummacher, T.D. Schmidt, W. Brtting, N. Danz, Oriented phosphorescent emitters boost OLED efficiency, Org. Electron. 12 (10) (2011) 1663–1668.

[10] W.M.V. Wan, N.C. Greenham, R.H. Friend, Interference effects in anisotropic optoelectronic devices, J. Appl. Phys. 87 (2000) 5.

[11] B. Ruhstaller, Polymer composite and multilayer organic light-emitting diodes, experiment and numerical simulation, PhD thesis, University of California, Santa Cruz, 2000.

[12] B. Perucco, N.A. Reinke, F. Müller, D. Rezzonico, B. Ruhstaller, The influence of the optical environment on the emission profile and methods of its determination, Proc. SPIE 7722 (2010) 14.

[13] B. Perucco, N.A. Reinke, D. Rezzonico, M. Moos, B. Ruhstaller, Analysis of the emission profile in organic light-emitting devices, Optics Express 18 (S2) (2010) A246–A260.

[14] B. Ruhstaller, T. Flatz, M. Moos, and G. Sartoris, Optoelectronic OLED modeling for device optimization and analysis, SID Symposium Digest of Technical Papers 38, 1686, 2007.

[15] M.C. Gather, M. Flämmich, N. Danz, D. Michaelis, K. Meerholz, Measuring the profile of the emission zone in polymeric organic light-emitting diodes, Appl. Phys. Lett. 94 (2009) 263301.

[16] H. Kuma, H. Tokairin, K. Fukuoka, C. Hosokawa, Optical simulation of OLED devices and its application for determination of emitting zone, SID 05 Digest 1279 (2005) 1276–1279.

[17] S.L.M. van Mensfoort, M. Carvelli, M. Megens, D. Wehenkel, M. Bartyzel, H. Greiner, R.A.J. Janssen, R. Coehoorn, Measuring the light emission profile in organic light-emitting diodes with nanometre spatial resolution, Nat. Photonics 4 (2010) 329–335.

[18] M. Carvelli, R.A.J. Janssen, R. Coehoorn, Spatial resolution of methods for measuring the light-emission profile in organic light-emitting diodes, J. Appl. Phys. 110 (2011) 8.

[19] A. Sommerfeld, Über die Ausbreitung der Wellen in der drahtlosen Telegraphie, Ann. D. Phys. 28 (1909) 665–736.

[20] R.R. Chance, A. Prock, R. Silbey, Molecular fluorescence and energy transfer near interfaces, Adv. Chem. Phys. 37 (1978).

[21] L. Novotny, Allowed and forbidden light in near-field optics. I.A single dipolar light source, J. Opt. Soc. Am. A 14 (1997) 91.

[22] K.A. Neyts, Simulation of light emission from thin-film microcavities, J. Opt. Soc. Am. A 15 (1998) 962.

[23] M. Flämmich, Optical characterization of OLED emitter properties by radiation pattern analyses, PhD thesis, Friedrich-Schiller-Universität Jena, 2011.

[24] B. Ruhstaller, S.A. Carter, S. Barth, H. Riel, W. Riess, J.C. Scott, Transient and steady-state behavior of space charges in multilayer organic light-emitting diodes, J. Appl. Phys. 98 (2001) 15.

[25] B. Ruhstaller, T. Beierlein, H. Riel, S. Karg, J.C. Scott, W. Riess, Simulating electronic and optical processes in multilayer organic light-emitting devices, IEEE J. Sel. Top. Quantum Electron. 9 (2003) 3.

[26] E. Knapp, R. Häusermann, H.U. Schwarzenbach, B. Ruhstaller, Numerical simulation of charge transport in disordered organic semiconductor devices, J. Appl. Phys. 108 (2010) 054504.

[27] Fluxim AG, Semiconducting emissive thin film optics simulator SETFOS, http://www.fluxim.com.

[28] M. Flämmich, M. C Gather, N. Danz, D. Michaelis, K. Meerholz, In situ measurement of the internal luminescence quantum efficiency in organic light-emitting diodes, Appl. Phys. Lett. 95 (2009) 263306.

[29] S. Harkema, R.A.H.J. Kicken, B.M.W. Langeveld-Voss, S.L.M. van Mensfoort, M.M. de Kok, R. Coehoorn, Tuning the voltage dependence of the efficiency of blue organic light-emitting diodes based on fluorene-amine copolymers, Org. Electron. 11 (5) (2010) 755–766.